Ultrafast excited-state dynamics in a prototype of the peptide bond: Internal conversion of the isolated N,N-dimethylformamide

Xuejun Qiu, Zhonghua Ding, Yanqi Xu, Yanmei Wang, and Bing Zhang*

State Key Laboratory of Magnetic Resonance and Atomic and Molecular Physics, Wuhan Institute of Physics and Mathematics, Chinese Academy of Sciences, Wuhan, Hubei 430071, People's Republic of China

and Graduate School of the Chinese Academy of Sciences, Beijing 100049, People's Republic of China

(Received 9 October 2013; published 6 March 2014)

A combination of femtosecond time-resolved photoelectron imaging technique and time-resolved mass spectroscopy technique are implemented to investigate the electronic excited-state dynamics in N,N-dimethylformamide (NNDMF). The ultrafast internal conversion (IC) of S_1 ($n\pi^*$) and S_2 ($\pi\pi^*$) excited states of NNDMF are observed in this experiment. The molecule is excited to the lowest-lying $^1\pi\pi^*$ state (S_2 state) following absorption of two 400-nm photons. It is found that the population of the S_2 ($\pi\pi^*$) state undergoes ultrafast IC to the highly vibrationally excited S_1 ($n\pi^*$) state within 99 fs by very fast C-N stretching, while the nonradiative deactivation of the S_1 ($n\pi^*$) state occurs in 2.4 ps, and it is to a large extent due to the C-N bond cleavage from the S_1 potential energy surface, which would be able to efficiently compete with the IC of $S_1 \rightarrow S_0$ through S_1/S_0 conical intersections.

DOI: 10.1103/PhysRevA.89.033405 PACS number(s): 33.50.Hv, 33.80.Eh, 33.60.+q

I. INTRODUCTION

Over the years peptide bond interactions with ultraviolet light have received considerable attention and have come to be regarded as a linkage in proteins that act as building blocks for many polymers. Knowledge of how they interact with ultraviolet light has important implications in such diverse fields as laser surgery and photodegradation of polymers [1]. There have been numerous spectroscopic studies carried out to investigate the N,N-dimethylformamide (NNDMF) [2–4], which is the simple prototype of the peptide bond. The $S_1 \leftarrow S_0$ transition is caused by a promotion of the O atom lone pair to the π^* antibonding orbital localized in the C=O group, assigned as the $n \rightarrow \pi^*$ excitation, and the promotion of a lone-pair $2p\pi$ electron on the N atom to the π^* antibonding orbital of the C=O group is assigned as the $S_2 \leftarrow S_0$ transition [4].

Investigations of photodissociation of NNDMF have also been extensively done in the past two decades. The early gas-phase experimental study was published by Butler and co-workers [5,6]. They found that the C-N bond cleavage proceeded along the excited-state pathway or through decay channel leading to fragments at 193 nm excitation to the second excited singlet state. Subsequently, Liu and co-workers [7] carried out complete active space self-consistent field calculations for the above proposed channels. The most probable mechanism, resulting in different products for the NNDMF photodissociation at 193 nm, was provided in their work. They pointed out that vibronic coupling between the S_2 and the S_1 electronic states played a significant role in the mechanism and dynamics of photodissociation of the C-N bond in NNDMF. The quantum of the C-N stretching is estimated to be 1200 cm^{-1} above the band origin of S_1 state. Recently Antol *et al.* studied the photodynamics of NNDMF in its low-lying singlet excited $n\pi^*$ and $\pi\pi^*$ states by the direct trajectory surface hopping method based on multiconfigurational *ab initio* calculations [8]. They proposed that the population of S_2 state decays to S_1 state through S_2/S_1 conical intersections (CI) by very fast C-N stretching. However, most of the population bypass the S_1/S_0 CI, because the C-N dissociation proceeds very fast in the S_2 state and continues in the S_1 state. Additionally, the lifetime of NNDMF in the S_1 and S_2 states is estimated to be 1 ps and 28 fs, respectively.

In the present work, we investigate the excited-state dynamics of NNDMF by the femtosecond time-resolved photoelectron imaging (TRPEI) technique, which has emerged as an extremely valuable tool for following excited-state dynamics in molecules [9–14]. In particular, it involves promoting an isolated molecule to an electronically excited state with an ultrashort pump pulse. A probe pulse then ionizes the excited state and the photoelectron images are recorded as a function of the pump-probe delay. One can gain further insight into the electronic and geometric changes along the reaction coordinate through TRPEI. In our results, the ultrafast IC from S_2 state to S_1 state have been experimentally confirmed, and the time scales of these internal conversion (IC) processes have been determined.

II. EXPERIMENT

TRPEI experiments were performed by combining a femtosecond laser system with the velocity map imaging apparatus, which has been described in detail elsewhere [15,16].

The vapor of NNDMF (99% purity) in equilibrium with 2 bars of He (about 0.18% NNDMF) was expanded through a 10-Hz pulsed electromagnetic valve to form a supersonic expansion. The collimated beam interacts with the femtosecond pulses generated by a Ti: sapphire oscillator regenerative amplifier system (1 kHz, 1 mJ, 35-fs pulses at 800 nm). The pump pulses were produced by doubling the fundamental beam in BBO crystals, and the 800-nm fundamental beam was chosen to probe the molecule. The bandwidths of pump and probe pulses were 4 and 30 nm, respectively. The theoretical cross-correlation time expected from these bandwidths was

*Author to whom correspondence should be addressed: bzhang@wipm.ac.cn

100 fs. The pulses were weakly focused into the interaction region by $f/300$ with 10.7 μJ/pulse for the pump pulse and 51.4 μJ/pulse for the probe pulse. The polarization states of the laser pulses were individually controlled by Berek compensators (New Focus) and set to orthogonal to the time-of-flight axis of the spectrometer.

The probe beam was optically delayed with respect to the pump beam using a motorized translation stage (PI, M-126.CG1). At each time delay, a sequence of accumulating photoelectron images due to pump + probe, pump only, and probe only were collected, the latter two being used for dynamic background subtraction. The acquisition time for each image was about 1 h. The images were inverted using a basis-set expansion (BASEX) transform [17] to calculate the slices through the three-dimensional (3D) scattering distributions of the photoelectrons from the observed 2D projection images. The energy scale of the velocity map imaging (VMI) detector was calibrated by $(2+1)$ resonant multiphoton ionization of I at 258.686 nm, to generate photoelectrons associated with the $^2P_{3/2}$ state of the atomic iodine. The energy resolution of the apparatus is 160 meV at 3 eV kinetic energy release.

III. RESULTS AND DISCUSSION

Two well-separated bands are observed in the absorption spectrum of NNDMF [2], one broad, intense band centered around 6.4 eV and a second, weak band at 5.5 eV. They correspond to the $S_2 \leftarrow S_0$ and $S_1 \leftarrow S_0$ transition; the 0-0 excitation energies of S_1 and S_2 can be estimated to be 5.4 and 6.0 eV from the absorption onset, respectively. In this experiment, the NNDMF molecule is excited into the S_2 state from its ground state S_0 by two photons of 400 nm, which is energetically equivalent to one-photon 200-nm excitation, then a probe pulse at 800 nm is used to probe relaxation dynamics of NNDMF from the S_2 state. The typical time-of-flight mass spectra (TOFMS) of NNDMF are recorded in the experiment, as displayed in Fig. 1. When only the pump laser or probe laser is present (top trace or center trace), the one-color signal is very small. When both lasers are present (bottom trace),

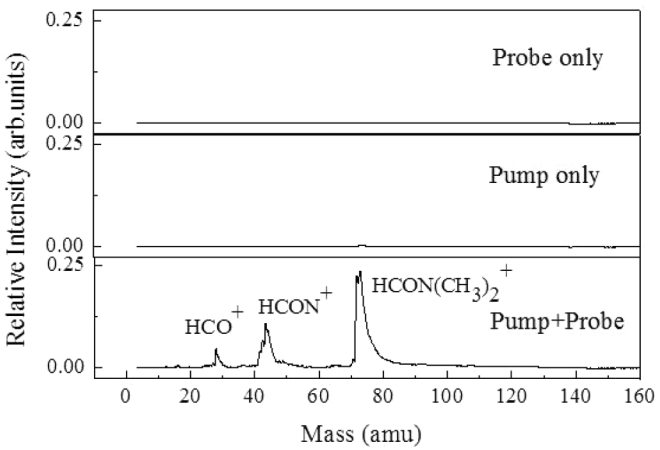

FIG. 1. Mass spectra of NNDMF illustrating the pump-probe contrast ratio achieved in the experiment. The pump-probe mass spectra are collected at $\Delta t = 42$ fs.

the NNDMF signal increases significantly, and yields three major peaks at $m/z = 73$, 43, and 29 amu, corresponding to $C_3H_7NO^+$, $HCON^+$, HCO^+, respectively; no cluster signal is observed from the TOFMS.

Figures 2(a)–2(d) show the temporal profiles obtained by monitoring the signal of the electron, $C_3H_7NO^+$, $HCON^+$, and HCO^+, respectively; each transient is collected in the focusing mode of VMI. However, the intensity of each pulse and the locations of the focus lens are adjusted to avoid the saturation of microchannel plate detectors, so the artifacts can be neglected for the cation transients in our experiment. The inset in Fig. 2(a) gives the cross-correlation width of about 110 fs by recording the temporal sum frequency signal of pump and probe pulses. The time zero point is determined by the cross-correlation peak of the sum frequency signal.

We fit these experimental data to a sum of exponentially decaying profiles convoluted with the cross correlation of the pump and probe laser pulses. The transient [Fig. 2(a)] for the electron is well described by a biexponential decay with $\tau_1 = 103$ fs and $\tau_2 = 2.8$ ps. The fitting results for the parent ion [Fig. 2(b)] signals present similar time constants as that of the electron, which implies that the photoelectrons are mostly from the ionization of the parent. The nascent fragments are produced by either direct photodissociation from a neutral molecule or the dissociative ionization. In the first case, the time dependence of these fragment signals depicted in Figs. 2(c) and 2(d) would level off at a nonzero constant value at later delays. According to our finding, the best fit for these fragments included only one constant, sub-100 fs, which is in good agreement with the fast component observed in the electron and parent ion time profiles. It seems that the direct photodissociation from a neutral molecule could be excluded. We will discuss these time constants in detail later through photoelectron images.

Figure 3 shows the photoelectron kinetic energy (PKE) spectrum at maximum intensity that is extracted from the corresponding BASEX-inverted images. The inset is the corresponding raw photoelectron image at $\Delta t = 42$ fs. The maximum electron kinetic energy available in $(2+2')$ and $(2+3')$ processes is indicated by the arrow, based on the adiabatic ionization energy, $D_0 = 9.12$ eV [18,19], of NNDMF. Five peaks are visible in the spectrum at 0.03, 0.65, 0.98, 1.35, and 1.60 eV. They are marked as the first, second, third, fourth, and fifth bands, respectively.

For $(2+2')$ process, the total energy would be 9.34 eV, i.e., only a little higher than D_0; the maximum electron energy is expected to be 0.22 eV. Therefore, most of the signal with high PKE in Fig. 3 corresponds to a three-photon probe process. Assuming that the 0.2 eV excess vibrational energy above S_2 state (6.0 eV) is conserved on ionization, one peak at about zero kinetic energy would appear for $(2+2')$ process, which is consistent with the observed first band. Note that the fifth band shows an energy spacing of 1.57 eV comparable to the first band, which is exactly the energy of one 800 nm photon. Thus, it is concluded that the first and fifth bands arise from the ionization of $D_0 \leftarrow S_2$ by two and three photons at 800 nm. Analogous to the previous discussion, the $(2+3')$ process provides a combined energy of 10.91 eV, i.e., above D_0 and D_1 (D_1 has an energy onset of 9.4 eV from gas-phase photoelectron spectra [18]). According to the

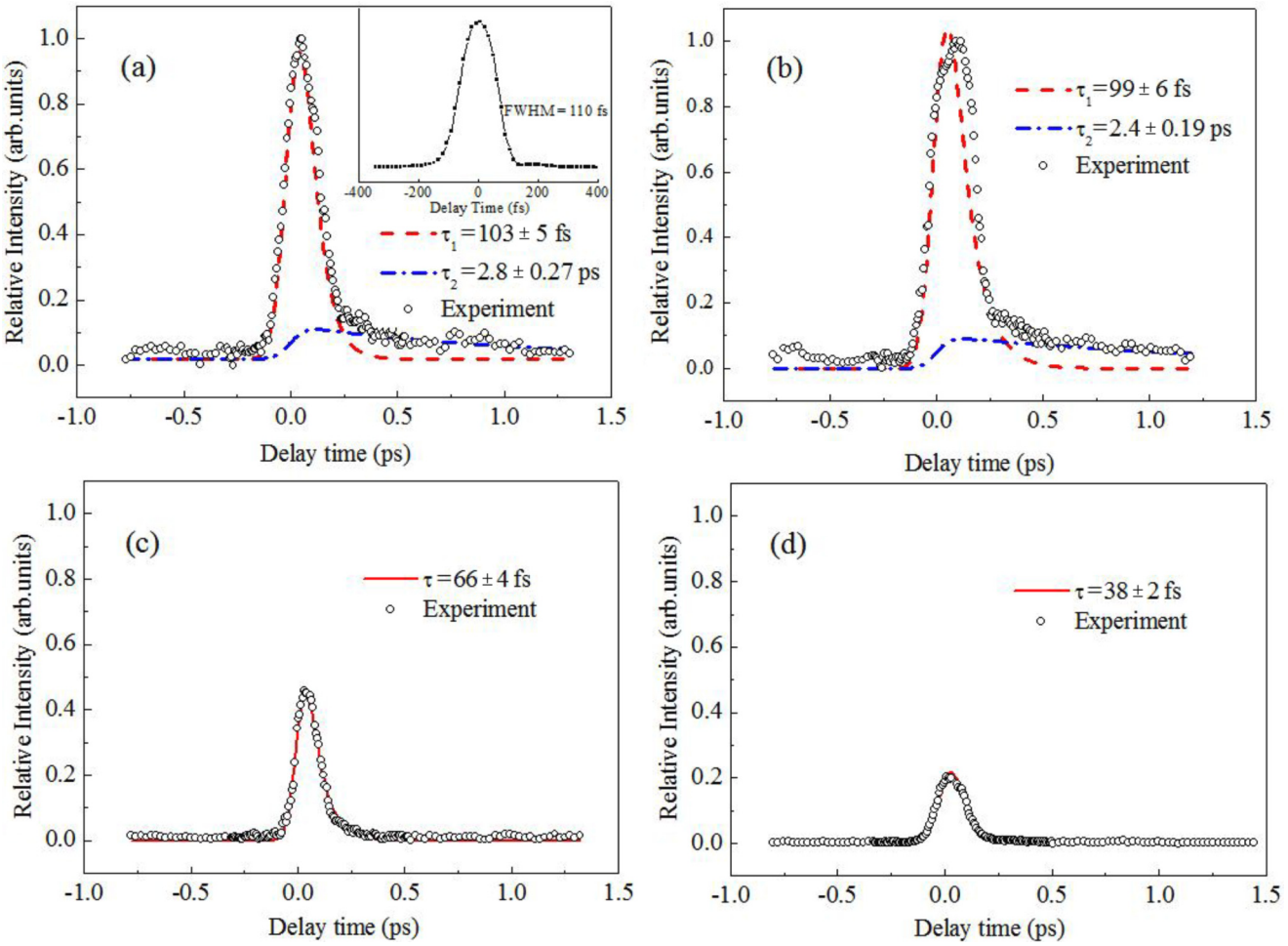

FIG. 2. (Color online) Decays recorded exciting in the 400 nm and probing with 800 nm pulses. Circles correspond to the experimental data, and dash and dash-dotted line are exponential fitting, panels (a)–(d) are temporal profiles obtained by monitoring the electron, and ion signal of $C_3H_7NO^+$, $HCON^+$, and HCO^+. The inset in panel (a) is the cross correlation acquired by recording the temporal sum frequency signal of pump and probe pulses.

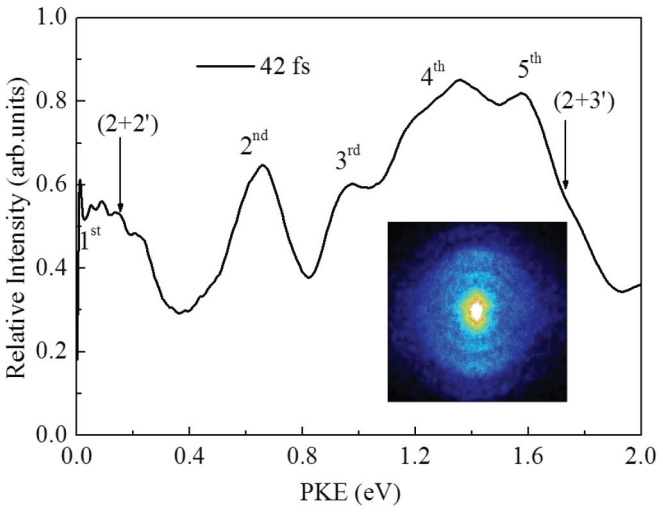

FIG. 3. (Color online) PKE spectrum extracted from the image at $\Delta t = 42$ fs. The inset is the corresponding raw photoelectron image data at 42-fs pump-probe delay.

$\Delta v = 0$ propensity rule, the fourth band located 1.35 eV can be assigned to $D_1 \leftarrow S_2$.

To interpret the various time constants from time profiles and understand other photoelectron bands, the time-dependent PKE distributions are extracted from a series of images, presented in Fig. 4. It reveals a fast decay for the energy below 0.22 eV (first band) and above 1.05 eV (fourth and fifth bands), whereas a shift to the second and third bands is evident in the time-energy distributions recorded at 120 fs, indicating a fast energy transfer from the first, fourth, and fifth bands to the second and third bands, which may be caused by the following possible dynamic mechanisms: (i) direct excitation to S_2 ($\pi\pi^*$) and passage toward the dissociation or isomerization; (ii) accessing the triplet state via spin-orbit coupling; (iii) coupling back to S_0 through the S_2/S_0 CI; and (iv) initial population of S_2 ($\pi\pi^*$) followed by rapid coupling onto S_1 ($n\pi^*$) through the S_2/S_1 CI. Liu *et al.* pointed out that the S_2 potential energy surface (PES) is repulsive with respect to the C-N bond, and the C-N bond cleavage would occur on a time scale of the C-N stretching vibration period after photoexcitation at 200 nm [7]. It is reasonable to conclude

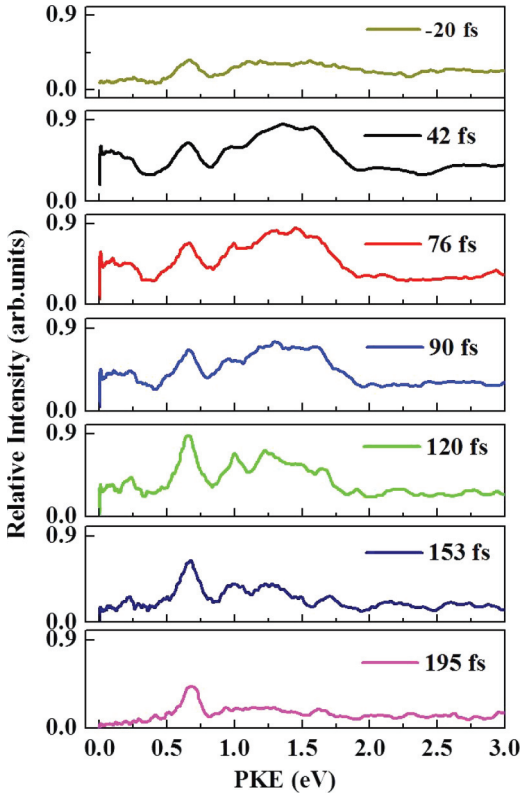

FIG. 4. (Color online) Time-dependent PKE distributions extracted from a series of images.

the time scale of intersystem crossing is longer than the dissociation or IC process, which leads to low quantum yields for S_2-T. We therefore tentatively propose that the dissociation or IC mechanism is the most feasible origin for the energy transfer in Fig. 4. However, the direct photodissociation signals from the excited molecule are not detected from the transients of fragments; we cannot give one conclusive presumption for this dynamic process. The alternative origin of the energy transfer could be from the IC toward S_1 or S_0. In light of the extremely poor Franck-Condon factor between the ground state with high vibrational levels and the cation states, the second and third bands are not possible from the ionization of the ground state.

With the aid of the electronic excitation energy of the S_1 state, we can assign the second and third bands. The gap between the S_1 and S_2 states is estimated to be 0.6 eV, which is in good agreement with the energy difference between the third and fifth bands, and the second and fourth bands in Fig. 3. The assignments of peak 2 and 3 to photoionization from the S_1 state are similar to the S_2 state based on the $dv = 0$ propensity rule of ionization; we therefore assigned the second and third bands as the ionization of $D_1 \leftarrow S_1$ and $D_0 \leftarrow S_1$, respectively. The lower intensity for $D_0 \leftarrow S_1$ shows that the limited Franck-Condon overlaps between S_1 and D_0. From this assignment, we are able to conclude that the shift to the second and third bands is induced by the main IC pathway via the S_2 PES of the molecule, which explains the first 99-fs time constant in the parent ion time profile, a notion supported by the calculated lifetime of NNDMF in the S_2 state [7]. The slow component mentioned above shows a time constant of $\tau_2 =$ 2.4 ps, which we can interpret as the decay time for the highly vibrationally excited S_1 state. As has been predicted by Liu *et al*. [7], most of the population would overshoot the S_1/S_0 CI and dissociate to form HCO and N $(CH_3)_2$ radicals, and the residual population would relax to the ground state PES and dissociate. A plausible explanation for the slow component is the C-N bond cleavage from the S_1 PES, which would be able to efficiently compete with the IC of $S_1 \rightarrow S_0$ through S_1/S_0 CI.

Upon close inspection of the PKE second and third bands, we found that they are all present at the longest delay, which might suggest a signature of the ionization from Rydberg states. To the best of our knowledge, there are two Rydberg states located between the S_1 and S_2 states, the $16a' \leftarrow 3s$ Rydberg transition and the $4a' \leftarrow 3s$ Rydberg transition, which are almost degenerate in energy. The $16a' \leftarrow 3s$ Rydberg transition is calculated to lie slightly lower compared with the S_2 state, by 0.08 eV at the complete active space level and by 0.02 eV at the second order perturbation level of theory [4], and the $4a' \leftarrow 3s$ Rydberg transition energy is determined to be 5.9 eV by experiment [2]. In our experiment, we cannot exclude the same time excitation of these Rydberg states and the S_2 state due to the similarity of energy. Therefore it may be that the photoelectron peak from the ionization of the S_2 state exhibits the ionization character of the Rydberg state, such as band 5. But for band 2, there is a big energy space (0.7 eV) between band 4 and band 2, which is in good agreement with the energy difference between the S_1 and S_2 state. The longer lifetime for band 2 reflects the slow photodissociation process

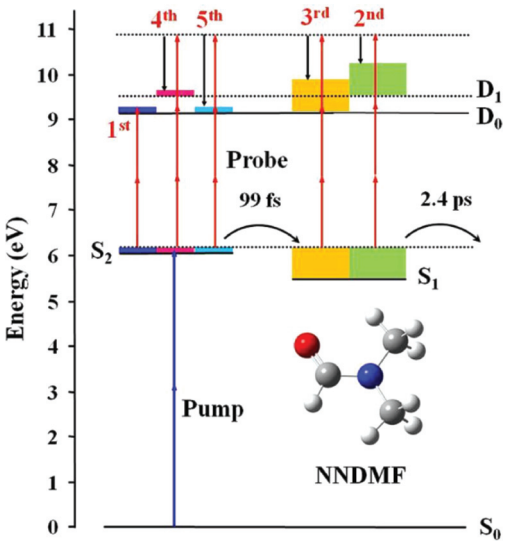

FIG. 5. (Color online) Excitation scheme. The 0-0 excitation energies of S_1 and S_2 are estimated to be 5.4 and 6.0 eV from the absorption onset [2,3], respectively. The 0-0 energies of the ground and first excited electronic states of the NNDMF cation have been determined to be 9.12 and 9.4 eV [18]. Assuming the $\Delta v = 0$ propensity rule, photoelectrons created by $(2+3')$ ionization process from S_1 and S_2 states in the vertical Franck-Condon region have PKE around 0.65, 0.98, 1.35, and 1.60 eV, respectively, while the $(2+2')$ ionization process from S_2 has PKE around zero.

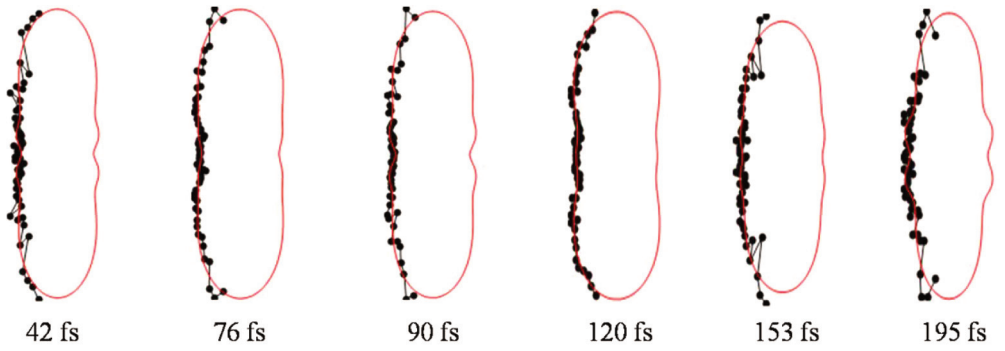

FIG. 6. (Color online) Polar plots of the PADs integrated for PKE of 0.9–1.7 eV at specified time delays, which is associated with ionization from the S_1 and S_2 states. Solid lines are theoretical fits. The linear polarizations of the pump and probe lasers are aligned vertically in the plane of the figure.

for the S_1 state, which is the same as the results calculated by Liu *et al*.

The time profiles collected at $m/z = 43$ amu and $m/z = 29$ amu show only one fast decay component. We have previously ascribed such signals to dissociative ionization; the lifetimes of the fragments correlate reasonably well with the deactivation of the S_2 state, implying that the fragments disappeared when the S_1 ($n\pi^*$) state is active via S_2/S_1 CI. Because the internal energy of the cation correlated with the S_1 state is larger than the S_2 state, it is likely that the parent ion would give other dissociated channels when the S_1 ($n\pi^*$) state is active via S_2/S_1 CI. However, no more fragments are observed in the mass spectra at longer delay time. One possible explanation is that the internal energy of the cation correlated to the S_1 state is allocated to other vibrational coordinates of the parent ion, but is not sufficient for realizing separation of the parent ion.

Thus far, the mechanism for the dynamics of the S_2 state can be briefly described, as shown in Fig. 5; after the initial promotion to the S_2 state, a fast 99-fs relaxation is observed, which correlates to the ultrafast IC from the S_2 to S_1 state through S_2/S_1 CI by very fast C-N stretching. Subsequently, the populated S_1 state decays via two pathways, the C-N bond cleavage from the S_1 PES and the IC to S_0. In our experiment, we cannot rule out the possible coexistence of the two interpretations of the $\tau_2 = 2.4$ ps component, if both mechanisms give rise to similar time constants.

Note also that in Fig. 4, the second and third bands show a smaller increase for the third band compared with the second band. This is mainly because photoionization from $D_0 \leftarrow S_1$ (third band) and $D_1 \leftarrow S_2$ (fourth band) overlap a lot in the PKE. In this case, photoelectron angular distributions (PADs) have been shown to provide an extremely sensitive probe of the time evolution of the electronic composition of the wave packets [20]. In our experimental configuration with the linear and parallel polarization of the pump and probe laser beams, the laboratory frame PADs following three-photon ionization can be expanded as [21]

$$I(\theta;t) = \sigma(t)[1 + \beta_2(t)P_2(\cos\theta) + \beta_4(t)P_4(\cos\theta) + \beta_6(t)P_6(\cos\theta) + \beta_8(t)P_8(\cos\theta) + \beta_{10}(t)P_{10}(\cos\theta)], \quad (1)$$

where $\sigma(t)$ is the integral cross section, $\beta_n(t)$ are the anisotropy parameters, $P_n(\cos\theta)$ are the Legendre polynomials, and θ is the angle between the laser polarization direction and the electron recoil direction. We find that the value from β_4 to β_{10} is negligible. The PADs correlated with the symmetry of the outgoing electron; once the symmetry of the outgoing electron changes, the symmetry of the initial excited state would also change in order to remain totally symmetric. Therefore the PADs are sensitive to changes of symmetry in the excited state. Figure 6 shows the polar plots of the PADs integrated for PKE of 0.9–1.7 eV at specified time delays, which is associated with ionization from the S_1 and S_2 states. The initial shapes of the PADs are almost the same when compared with each other, and then they change dramatically as the delay time changes; these changes can be clearly characterized by the values of β_2, as shown in Table I. We find the β_2 value changes gradually from 0.85 ($\Delta t = 42$ fs) to 0.58 ($\Delta t = 195$ fs), which indicates that the initial component of the electronic wave packets is mainly in S_2 ($^1A'$) symmetrical character and then evolves into the mixing of S_2 ($^1A'$) and S_1 ($^1A''$) symmetrical characters through the IC of $S_2 \rightarrow S_1$.

IV. CONCLUSIONS

The reported time domain experiments with femtosecond resolution provide insights into the rich photophysics of the NNDMF molecule. The electronic relaxation of the molecules is driven for the interplay of at least three singlet electronic states S_0, S_1, and S_2. The ultrafast IC of the S_2 state toward

TABLE I. The time-dependent β_2 value for PKE of 0.9–1.7 eV.

Delay	42 fs	76 fs	90 fs	120 fs	153 fs	195 fs
β_2	0.851 ± 0.002	0.843 ± 0.006	0.819 ± 0.01	0.773 ± 0.002	0.667 ± 0.01	0.581 ± 0.01

the higher S_1 state is detected through femtosecond TRPEI coupled with time-resolved mass spectroscopy. The 99-fs time constant measured from the parent ion time profile points to the IC involvement of S_2/S_1 CI by very fast C-N stretching. The slow component, occurring at 2.4 ps, is attributed to the competition between photodissociation from the S_1 PES and the IC of $S_1 \rightarrow S_0$ through S_1/S_0 CI. The formation of the fragments in the mass spectrum originates from the dissociative ionization of the cationic state. Our results not only provide insights into the understanding of the dissociation mechanism in the NNDMF, but also would be quite significant to relevant theoretical study that aims at describing these electronic dephasing processes.

ACKNOWLEDGMENTS

This work was supported by National Basic Research Program of China (973 Program) (Grant No. 2013CB922200), and National Natural Science Foundation of China (Grants No. 91121006, No. 21273274, and No. 21173256).

[1] A. Sionkowska, J. Photochem. Photobiol. A **117**, 61 (2006).
[2] H. D. Hunt and W. T. Simpson, J. Am. Chem. Soc. **75**, 4540 (1953).
[3] K. Kaya and S. Nakagura, Theor. Chim. Acta. **7**, 117 (1967).
[4] L. Serrano-Andres and M. P. Fulscher, J. Am. Chem. Soc. **118**, 12190 (1996).
[5] N. R. Forde, T. L. Myers, and L. J. Butler, Faraday Discuss. **108**, 221 (1997).
[6] N. R. Forde, L. J. Butler, and S. A. Abrash, J. Chem. Phys. **110**, 8954 (1999).
[7] D. Liu, W. H. Fang, Z. Y. Lin, and X. Y. Fu, J. Chem. Phys. **117**, 9241 (2002).
[8] M. Eckert-Maksic and I. Antol, J. Phys. Chem. A. **113**, 12582 (2009).
[9] B. Kim, C. P. Schick, and P. M. Weber, J. Chem. Phys. **103**, 6903 (1995).
[10] R. S. Minns, D. S. N. Parker, T. J. Penfold, G. A. Worth, and H. H. Fielding, Phys. Chem. Chem. Phys. **12**, 15607 (2010).
[11] D. S. N. Parker, R. S. Minns, T. J. Penfold, G. A. Worth, and H. H. Fielding, Chem. Phys. Lett. **469**, 43 (2009).
[12] V. Blanchet, M. Z. Zgierski, T. Seideman, and A. Stolow, Nature **401**, 52 (1999).
[13] G. M. Roberts, C. A. Williams, J. D. Young, S. Ullrich, M. J. Paterson, and V. G. Stavros, J. Am. Chem. Soc. **134**, 12578 (2012).
[14] D. A. Horke and J. R. R. Verlet, Phys. Chem. Chem. Phys. **13**, 19546 (2011).
[15] J. Long, C. Qin, Y. Liu, S. Zhang, and B. Zhang, Phys. Rev. A **84**, 063409 (2011).
[16] C. C. Qin, Y. Z. Liu, S. Zhang, Y. M. Wang, Y. Tang, and B. Zhang, Phys. Rev. A **83**, 033423 (2011).
[17] V. Dribinski, A. Ossadtchi, V. A. Mandelshtam, and H. Reisler, Rev. Sci. Instrum. **73**, 2634 (2002).
[18] C. R. Brundle, D. W. Turner, M. B. Robin, and H. Basch, Chem. Phys. Lett. **3**, 292 (1969).
[19] K. Watanabe, T. Nakayama, and J. Mottl, J. Quant. Spectrosc. Radiat. Transfer **2**, 369 (1962).
[20] T. Horio, T. Fuji, Y. I. Suzuki, and T. Suzuki, J. Am. Chem. Soc. **131**, 10392 (2009).
[21] C. N. Yang, Phys. Rev. **74**, 764 (1948).